SUPPLEMENTARY INFORMATION
Self-testing of a single quantum system from theory to experiment

Xiao-Min Hu,[1, 2, 3] Yi Xie,[4, 5] Atul Singh Arora,[6, 7] Ming-Zhong Ai,[1, 2, 3] Kishor Bharti,[8, 9, 10] Jie Zhang,[4, 5] Wei Wu,[4, 5, 11] Ping-Xing Chen,[4, 5, 11, *] Jin-Ming Cui,[1, 2, 3] Bi-Heng Liu,[1, 2, 3, *] Yun-Feng Huang,[1, 2, 3, *] Chuan-Feng Li,[1, 2, 3] Guang-Can Guo,[1, 2, 3] Jérémie Roland,[6] Adán Cabello,[12, 13, *] and Leong-Chuan Kwek[8, 14, 15, *]

[1] *CAS Key Laboratory of Quantum Information, University of Science and Technology of China, Hefei, 230026, China*
[2] *CAS Center For Excellence in Quantum Information and Quantum Physics, University of Science and Technology of China, Hefei, 230026, China*
[3] *Hefei National Laboratory, University of Science and Technology of China, Hefei, 230088, China*
[4] *Department of Physics, College of Liberal Arts and Sciences, National University of Defense Technology, Changsha 410073, Hunan, China*
[5] *Hunan Key Laboratory of Mechanism and Technology of Quantum Information, Changsha Hunan 410073, China*
[6] *Centre for Quantum Information & Communication, Université libre de Bruxelles, B-1050 Bruxelles, Belgium*
[7] *Institute of Quantum Information and Matter, Department of Computing and Mathematical Sciences, California Institute of Technology, USA*
[8] *Centre for Quantum Technologies, National University of Singapore, Singapore*
[9] *Joint Center for Quantum Information and Computer Science and Joint Quantum Institute, NIST/University of Maryland, College Park, Maryland 20742, USA*
[10] *Institute of High Performance Computing, Agency for Science, Technology and Research (A*STAR), 1 Fusionopolis Way, Connexis, Singapore 138632, Singapore*
[11] *Hefei National Laboratory, Hefei 230088, PR China*
[12] *Departamento de Física Aplicada II, Universidad de Sevilla, E-41012 Sevilla, Spain*
[13] *Instituto Carlos I de Física Teórica y Computacional, Universidad de Sevilla, E-41012 Sevilla, Spain*
[14] *MajuLab, CNRS-UNS-NUS-NTU International Joint Research Unit, Singapore UMI 3654, Singapore*
[15] *National Institute of Education, Nanyang Technological University, Singapore 637616, Singapore*

SUPPLEMENTARY NOTE 1 (QUANTIFICATION OF NOISE)

We look at three sources of deviation from our assumption—KCBS orthogonality (stated as Assumption 1 in the main text), Perfect Detection (no post-selection) and Random Selection of Measurements (the experimenter is not correlated with the state being measured). We implicitly made the last two assumptions in our analysis. *Perfect detection* was assumed because our measurements were projective and do not allow for events where the measurement itself fails. Allowing for such a possibility amounts to post-selection which in turn allows non-contextual (classical) models to also violate the classical bound and therefore no self-test guarantees can be made in that case. We also assumed that the actions of the observer and the (quantum) state are uncorrelated. If such correlations are allowed, then the aforementioned issue again nullifies any self-test guarantees. *Random Selection of Measurements* helps address this concern to some extent (we do not discuss this further as this has been widely studied in the Bell nonlocality setting).

KCBS orthogonality. Our theoretical analysis only applies for experiments which satisfy the KCBS orthogonality condition, i.e., Assumption 1 in the main text. To simplify the discussion, we use Π_i to denote $\Pi_{1|i}$. We slightly abuse the notation and use Π_i to denote the measurement itself as well. While it is impossible to perfectly satisfy Assumption

---

[*] pxchen@nudt.edu.cn, bhliu@ustc.edu.cn, hyf@ustc.edu.cn, adan@us.es, kwekleongchuan@nus.edu.sg

The first five authors contributed equally to this work.

1 in practice, our experiment comes close. Since we assume our measurements Π_i to be *projective*, they satisfy $\Pi_i^2 = \Pi_i$. This in particular entails *repeatability* at the level of observed statistics, $\langle \Pi_i^2 \rangle = \langle \Pi_i \rangle$, i.e., the same measurement repeated twice should give the same result for a fixed state, which we quantify by considering

$$R_i := \Pr(00|ii) + \Pr(11|ii), \tag{1}$$

where $\Pr(ab|ij)$ is the probability of obtaining outcomes (a, b) when first Π_i is measured, followed by Π_j as defined in the main text. Corresponding to various measurement settings in different experimental configurations, the repeatability in our experiment has been tabulated as Supplementary Tables VIII, IX and X. We find that the mean repeatability of our measurements for the entire experimental dataset is $\mu = 0.994217$ with standard deviation $\sigma = 0.00015985$.

We also assumed that our measurements Π_i are cyclically *orthogonal*, i.e., $\Pi_i \cdot \Pi_j = 0$ whenever $(i, j) \in E$. At the level of experimental statistics, this entails that

1. $\Pr(11|ij) = \Pr(11|ji) = 0$. This follows from the fact that $\langle \Pi_i \Pi_j \rangle = \langle \Pi_j \Pi_i \rangle = 0$.
2. $\Pr(10|ij) = \Pr(01|ji)$. This follows from the fact that $\langle \Pi_i (\mathbb{I} - \Pi_j) \rangle = \langle (\mathbb{I} - \Pi_j) \Pi_i \rangle$.
3. $\Pr(01|ij) = \Pr(10|ji)$. This follows from the fact that $\langle \Pi_j (\mathbb{I} - \Pi_i) \rangle = \langle (\mathbb{I} - \Pi_i) \Pi_j \rangle$.
4. $\Pr(00|ij) = \Pr(00|ji)$. This follows from the fact that $\langle (\mathbb{I} - \Pi_i)(\mathbb{I} - \Pi_j) \rangle = \langle (\mathbb{I} - \Pi_i)(\mathbb{I} - \Pi_j) \rangle$.

To quantify the deviations from *orthogonality* in the experimental data for projectors $\Pi_i$and Π_j, we use the following two quantities:

$$\delta_{ij} = \sum_{a,b \in \{0,1\}} |\Pr(ab|ij) - \Pr(ba|ji)|, \tag{2}$$

and

$$o_{ij} := p(11|ij). \tag{3}$$

Deferring the individual estimates of δ_{ij} and o_{ij} to Supplementary Tables IV and V, respectively, we report their mean and standard deviation averaged over all i, j: $\delta = 0.016 \pm 0.012$ and $o = 0.000550 \pm 0.0000984$.

Perfect detection. A quantum jump detection is used to detect the probability in $|S_{1/2}\rangle$, which is the "bright state". The photons that radiate from the ion are collected through two objectives each with numerical aperture around NA = 0.32. In this experiment, we use two different settings of the detection laser for the first and second photon detection steps. In the first detection step, the frequency of 397 nm laser is red detuned by half the natural linewidth and the laser intensity is set to lower level to minimize the heating effect, and the detection time is suppressed to 220 μs to minimize the random phase accumulation and decoherence. We observe on average 12 photons for the state $|0\rangle$ and less than 2.5 photons for the state $|1\rangle$ or $|2\rangle$. That is to say, the threshold value to distinguish bright state and dark state is set to $n_{ph} = 2.5$. The state detection error rates for wrongly registering the state $|0\rangle$ and missing the state $|0\rangle$ are 0.07% and 0.2%, respectively. For the second detection step, the laser frequency is set to on resonance. Together with 6 times higher laser power and 300 μs detection time, detection error is further suppressed. We observe on average 41 photons for the state $|0\rangle$ and 0.3 photons for the state $|1\rangle$ or $|2\rangle$. By setting the threshold to $n_{ph} = 8.5$, the state detection error rates for wrongly registering the state $|0\rangle$ and missing the state $|0\rangle$ are far less than 0.04%. Since the detection efficiency of the ion trap is close to 100%, our detection is nearly perfect.

Random selection of measurements. The choice of observables to measure is made randomly in our experiment using a quantum random number generator (QRNG). Before each measurement, we prepare the ions to the $|0\rangle$ state. First, a random integer m between 1 and 10 is generated. The random number $i = m \mod 5$ selects an observable Π_i from $\{\Pi_1, \Pi_2, \ldots, \Pi_5\}$, with Π_0 equal to Π_5, Then, one of the two observables $\Pi_{i\pm1}$ which are compatible with Π_i is selected randomly by the sign of $5.5 - m$. The random integer from the RNG determining control sequences are updated in real time (pregenerated before every experiment).

Relation with prior contextuality experiments

To the best of our knowledge, in all previous experiments on contextuality, an operational approach was taken. This approach is of interest because for foundational questions, one must phrase the necessary assumptions in a theory-independent language. Our experiment may also be charactarised in this language—demonstration of perfect detection addresses *the detection loophole* while the random selection of measurements addresses *the free choice loophole*. We already saw a brief description of these loopholes. We now state the analogue of our KCBS orthogonality condition. At the operational level, the notion of contextuality is usually defined for a set of *sharp* measurements which satisfy some *compatiblity* relation among them. We briefly review their definitions.

Sharp measurements are repeatable and minimally disturbing—any measurement compatible with it should yield the same output distribution regardless of whether it was measured or not. It is easy to see that sharp measurements imply, in particular, that $R_i = 1$ and $\delta_{ij} = 0$. Our data therefore also serves as evidence for sharpness of measurements.

Compatibility. Two observables are compatible if they can be jointly measured. In case the observables are measured sequentially, this implies that the order in which they are measured does not matter. Again, it is easily seen that this would entail $\delta_{ij} = 0$. Our data, as discussed above, supports the conclusion that our measurements are targeting compatible observables (corresponding to the five cycle graph).One might wonder how compatibility and sharpness are different (aside from the repeatability aspect). The difference is that for sharpness, the non-disturbance condition must hold for all compatible observables. The compatibility condition may only require one to verify a subset of these observables to be compatible.

SUPPLEMENTARY NOTE 2 (EXPERIMENTAL DATAPOINTS TO ASSESS REPEATABILITY AND ORTHOGONALITY)

In this section, we present the details for repeatability and orthogonality corresponding to various measurement settings in different experiments. See Supplementary Tables I, II and III for details regarding repeatability. For orthogonality, refer to Supplementary Tables IV and V.

Repeatability	μ	σ
R_1	0.994	0.001
R_2	0.991	0.002
R_3	0.990	0.002
R_4	0.993	0.001
R_5	0.994	0.001

Supplementary Table I: The above Table shows the repeatability of the measurements corresponding to the first set of experiments. For every data-point, we collect 14999 samples.

Repeatability	μ	σ
R_1	0.999	0.002
R_2	0.995	0.001
R_3	0.996	0.001
R_4	0.992	0.001
R_5	0.992	0.002

Supplementary Table II: The above Table shows the repeatability of the measurements corresponding to the second set of experiments for $\theta = 150.612$. Zero standard deviation in some of the cases appear due to rounding up to three digits after decimal. For every data-point, we collect 14999 samples.

Repeatability	μ	σ
R_1	0.999	0.001
R_2	0.996	0.001
R_3	0.999	0.002
R_4	0.992	0.001
R_5	0.994	0.001

Supplementary Table III: The above Table shows the repeatability of the measurements corresponding to the second set of experiments for $\theta = 22.041$. Zero standard deviation in some of the cases appear due to rounding up to three digits after decimal. For every data-point, we collect 14999 samples.

Configuration	$\mu = 10^{-2}\times$	$\sigma = 10^{-2}\times$
$p = 0$, N	0.500	0.024
$p = 0$, R	0.819	0.040
$p = 0.1$, N	0.875	0.040
$p = 0.1$, R	0.802	0.038
$p = 0.2$, N	0.801	0.040
$p = 0.2$, R	0.667	0.353
$\theta = 22.041$, N	0.385	0.027
$\theta = 22.041$, R	0.305	0.024
$\theta = 150.612$, N	0.210	0.020
$\theta = 150.612$, R	0.198	0.019

Supplementary Table IV: The above table summarizes the deviation from orthogonality (quantified via o_{ij} for measurements i and j) for various experiments. We present the mean μ and standard deviation σ for the set of values $\{o_{ij}\}_{i=1}^{5}$, where $j = i + 1$. Here, "Configuration" refers to various experimental settings as discussed in the paper. In the configuration column, "N" and "R" represent normal and reverse order.

Configuration	δ_{12}	δ_{23}	δ_{34}	δ_{45}	δ_{51}	μ	σ
$p = 0$	0.014	0.030	0.017	0.027	0.003	0.018	0.010
$p = 0.1$	0.019	0.014	0.017	0.013	0.010	0.015	0.003
$p = 0.2$	0.008	0.011	0.023	0.018	0.023	0.017	0.006
$\theta = 22.041$	0.006	0.011	0.029	0.010	0.004	0.012	0.009
$\theta = 150.612$	0.008	0.008	0.010	0.008	0.008	0.008	0.001
Overall	0.007	0.005	0.022	0.037	0.009	0.016	0.012

Supplementary Table V: The above table shows the possible values of δ_{ij} for different experimental configuration. Intuitively speaking, δ_{ij} captures the difference in statistics for normal and reverse order experiments.

SUPPLEMENTARY NOTE 3 (STATE AND MEASUREMENT TOMOGRAPHY)

In this section, we discuss the experimental process involved towards measurement and state tomography. We prepare the initial state in the $|0\rangle$ state with 10 μs optical pumping. In order to find the fidelity of this initial state, we did state tomography according to the Ref. [1]. As for a qutrit, we can write the density matrix as $\rho = \frac{1}{3}\sum_{j=0}^{8} r_j \lambda_j$, where the λ_j are the SU(3) generators and identity operator λ_0. The measurement basis $\{|\psi_j\rangle\}$ used in state tomography are chosen to be $|0\rangle$, $|1\rangle$, $|2\rangle$, $(|0\rangle + |1\rangle)/\sqrt{2}$, $(|0\rangle + i\,|1\rangle)/\sqrt{2}$, $(|0\rangle + |2\rangle)/\sqrt{2}$, $(|0\rangle + i\,|2\rangle)/\sqrt{2}$, $(|1\rangle + |2\rangle)/\sqrt{2}$, $(|1\rangle + i\,|2\rangle)/\sqrt{2}$, and we use the projection operator $|\psi_j\rangle\langle\psi_j|$ as the generators. All the results are shown in Supplementary Tables VI and VII.

We did measurement tomography according to Ref. [2]. The probability p_{lm} that the apparatus will respond with positive operator-values measure (POVM) Π_l when measuring the quantum state with density matrix can be expressed as $p_{lm} = \mathrm{tr}[\Pi_l \rho_m]$, where tr stands for the trace. Assuming that the theoretical detection probability p_{lm} can be replaced with relative experimental frequency f_{lm}, we may write $\mathrm{Tr}[\Pi_l \rho_m] = \sum_{i,j=1}^{N} \Pi_{l,ij}\rho_{m,ji} = f_{lm}$, where N is the dimension of Hilbert space on which the operators Π_l act. Then we can reconstruct the POVM Π_l according to experimental result f_{lm}. The density matrix ρ_m chosen in this process are the same as projection operators $|\psi_j\rangle\langle\psi_j|$ in state tomography. Also the maximum likelihood estimation (MLE) method is used in this process to ensure $\Pi_l \geqslant 0$ and $\sum_{l=1}^{k}\Pi_l = I$, where k is the number of measurement outcomes. The results are shown in Supplementary Tables VIII, IX and X.

SUPPLEMENTARY NOTE 4 (FIDELITY LOWER BOUND IN THE SECOND SET OF EXPERIMENTS)

The trace distance between two matrices A and B is given by $D(A,B) = \frac{1}{2}\|A-B\|_{tr}$, where $\|\|_{tr}$ denotes the trace norm. If A and B are density matrices, then we have the following lower and upper bounds on the trace distance in terms of fidelity,

$$1 - \sqrt{F(A,B)} \leq D(A,B) \leq \sqrt{1 - F(A,B)}. \tag{4}$$

After applying traingle inequality for density matrices A, B and C gives

$$1 - \sqrt{F(A,C)} \leq D(A,C) \leq D(A,B) + D(B,C) \leq \sqrt{1 - F(A,B)} + \sqrt{1 - F(B,C)}. \tag{5}$$

This gives a version of “traingle inequality for fidelity,”

$$\sqrt{F(A,C)} \geq 1 - \sqrt{1-F(A,B)} - \sqrt{1-F(B,C)}. \tag{6}$$

If at least one of the states among A and C is a pure state, one can tighten the lower bound on $D(A,C)$,

$$1 - F(A,C) \leq D(A,C). \tag{7}$$

Thus, we have

$$F(A,C) \geq 1 - \sqrt{1-F(A,B)} - \sqrt{1-F(B,C)}. \tag{8}$$

We use inequality 8 to relate the total fidelity of the experimental configuration $(\rho^E, \{\Pi_i^E\})$ to an optimal configuration $(|u_0^O\rangle\langle u_0^O|, \{|u_i^O\rangle\langle u_i^O|\}_i)$. Let us denote the fidelity of the experimental configuration to $|u_i^O\rangle$ as $F_i^{E,O}$. Similarly other fidelities are denoted by $F_i^{E,\theta}$ and $F_i^{\theta,O}$. It is easy to see the following lower bound on the total fidelity $\left(\sum_{i=0}^5 F_i^{E,O}\right)$:

$$\sum_{i=0}^{5} F_i^{E,O} \geq 6 - \left(\sum_{i=0}^{5}\sqrt{1-F_i^{E,\theta}}\right) - \left(\sum_{i=0}^{5}\sqrt{1-F_i^{\theta,O}}\right). \tag{9}$$

SUPPLEMENTARY NOTE 5 (FURTHER DETAILS ABOUT THE EXPERIMENTAL DATA)

In this section, we discuss further details regarding the experimental data. In Supplementary Figure 1, we present the data corresponding to the reverse order experiments. The fidelity of the prepared quantum state to the state to be prepared is shown in Supplementary Tables VI and VII. For the first set of experiments corresponding to $\theta = 48$, the fidelity of the implemented projector to the the projector to be implemented has been shown in Supplementary Table VIII. For the second set of experiments corresponding to Equation III.14 and Equation III.15 in the main text, the corresponding fidelities has been shown in Supplementary Tables IX and X.

State	Fidelity to self	Fidelity to $\|0\rangle$
$\|0\rangle$	0.999 $\pm$0.008	0.999 $\pm$ 0.008
$\|1\rangle$	0.999 $\pm$0.006	0.004 $\pm$ 0.002
$\|2\rangle$	0.993 $\pm$ 0.012	0.005 $\pm$ 0.002
Mixed with $p = 0.1$	0.996 $\pm$ 0.010	0.935$\pm$ 0.008
Mixed with $p = 0.2$	0.992 $\pm$ 0.008	0.846 $\pm$ 0.013

Supplementary Table VI: The above table shows the fidelity of the prepared state to the fidelity of the state to be prepared (the state $|0\rangle$) in row 1,4 and 5. Here, the state with mixedness p represents the density matrix $\rho'(p) = (1-p)|0\rangle\langle 0| + \frac{p}{9}\mathbb{I}$. The numbers after $\pm$ represent the standard deviation values. The data in row 2 and 3 is for sanity check, i.e, the state state $|1\rangle$ and $|2\rangle$ should be orthogonal to the state $|0\rangle$. For every data-point, we collect 4000 samples.

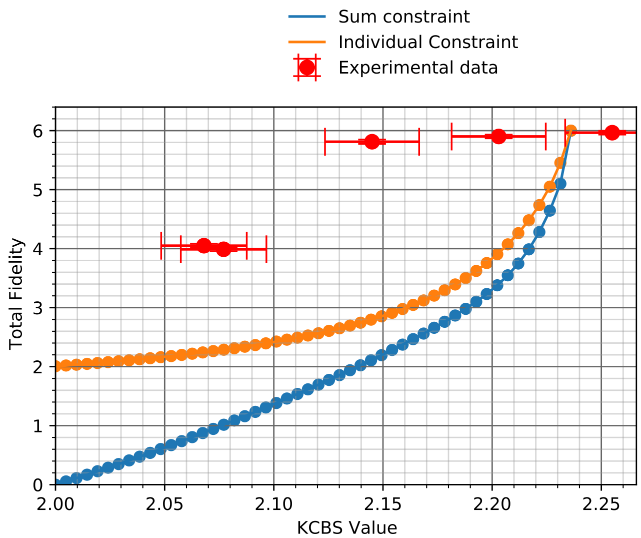

Supplementary Figure 1: The above plot is the analog of Figure I.1 (see main text) corresponding to the data obtained via reverse ordered experiments.

State	Fidelity	σ
$\theta = 22.041$	0.994	0.008
$\theta = 150.612$	0.995	0.009

Supplementary Table VII: The above table shows the fidelity of the experimentally prepared state to the state to be prepared corresponding to Equation III.14 and Equation III.15 in the main text. For every data-point, we collect 4000 samples.

Measurements	Fidelity	σ
Π_1	0.993	0.006
Π_2	0.991	0.006
Π_3	0.996	0.004
Π_4	0.995	0.006
Π_5	0.990	0.009

Supplementary Table VIII: The above table shows the fidelity of the experimentally implemented projectors to the projectors to be implemented corresponding to the first set of experiments. For every data-point, we collect 15000 samples.

SUPPLEMENTARY NOTE 6 (RELATION TO PRIOR WORK)

Comparison to another single system self-testing scheme. In a breakthrough result, a self-testing scheme for a single quantum system was introduced by [3] which relied on cryptographic assumptions, instead of no-communication (as in

Measurements	Fidelity	σ
Π_1	0.997	0.004
Π_2	0.998	0.005
Π_3	0.997	0.005
Π_4	1.000	0.007
Π_5	0.997	0.006

Supplementary Table IX: The above table shows the fidelity of the experimentally implemented projectors to the projectors to be implemented corresponding to the second set of experiments for $\theta = 22.041$. For every data-point, we collect 15000 samples.

Measurements	Fidelity	σ
Π_1	0.995	0.004
Π_2	0.995	0.007
Π_3	0.994	0.005
Π_4	0.996	0.005
Π_5	0.993	0.005

Supplementary Table X: The above table shows the fidelity of the experimentally implemented projectors to the projectors to be implemented corresponding to the second set of experiments for $\theta = 150.612$. For every data-point, we collect 15000 samples.

the Bell case) or some requirement on the measurements (as in the case of contextuality). Arguably, this approach makes a qualitatively weaker assumption about the device. Yet, despite the theoretical appeal, they remain elusive with current technologies—the cryptographic functions involved in such schemes, seem to require at least 1,000 qubits which need to be held coherent for about 10,000 layers of gates (estimate based on [4]). This limitation is circumvented by our contextuality based self-test which can be already be implemented on a qutrit (viz. a three-level system). (The number of qubits serves as the security parameter; higher the number, harder it is for a classical machine to break the underlying cryptographic scheme. The estimate ensures today's classical computers will not be able to break the scheme. Proof of principle experiments may be possible with fewer qubits but they may be seen as having "computational loopholes"—classical computers will be able to spoof such tests.)

Comparison to other works on contextuality. Works on contextuality conventionally use an operational (i.e. theory independent) language to formulate the associated concepts. In this work, however, we take a more pragmatic approach and work directly under the assumption that quantum mechanics governs the behaviour of our devices. Consequently, the terminology we use to characterise our experiment is slightly different from prior works. More precisely, the analogue of our KCBS orthogonality requirement, in the operational perspective may be thought of as compatibility and sharpness of measurements (see Supplementary Note 1).

[1] RT Thew, Kae Nemoto, Andrew G White, and William J Munro. Qudit quantum-state tomography. *Phys. Rev. A*, 66(1):012303, 2002.
[2] Jaromír Fiurášek. Maximum-likelihood estimation of quantum measurement. *Phys. Rev. A*, 64(2):024102, 2001.
[3] Tony Metger and Thomas Vidick. Self-testing of a single quantum device under computational assumptions. *Preprint at arXiv:2001.09161*, 2020.
[4] Gregory D Kahanamoku-Meyer, Soonwon Choi, Umesh V Vazirani, and Norman Y Yao. Classically-verifiable quantum advantage from a computational bell test. *Preprint at arXiv:2104.00687*, 2021.